JOURNAL OF SOLID STATE CHEMISTRY 57, 178–190 (1985)

Structure and Morphology Study of the Metastable Q_2 Form in $LiFeO_2$ Ferrite by X-Ray Diffraction and Transmission Electron Microscopy

R. FAMERY, P. BASSOUL, AND F. QUEYROUX

Laboratoire de Chimie du Solide Minéral, ERA 912, ESPCI—10, rue Vauquelin, 75231 Paris Cedex 05, France

Received June 11, 1984; in revised form September 10, 1984

Two periodic antiphase models of the Q_2 form structure were reported a few years ago. The use of complementary techniques (X-ray diffraction and transmission electron microscopy) to investigate Q_2 form single crystals, has allowed the selection of only one model. From its structural characteristic features (space group $C2/c$, one direction of modulation) and from the study of habit planes between the observed families of twins, a complete interpretation of the complex twinning is given. It can be explained by the existence of 48 variants. This interpretation is discussed and validated since a calculation of the reciprocal reflection positions for the 48 variants is in good agreement with the observed particularities in X-ray diffraction patterns. © 1985 Academic Press, Inc.

A. Introduction

There are three forms in lithium ferrite:

—A disordered C_1 form, cubic with a NaCl-type structure and $Fm3m$ space group, stable above 670°C, $a_{C_1} = 4.157$ Å (*1*).

—An ordered Q_1 form, tetragonal with $I4_1/amd$ space group, stable below 670°C, $a_{Q_1} = 4.045$ Å and $c_{Q_1} = 8.75$ Å (*2*).

—A metastable Q_2 form, the formation of which precedes the formation of stable Q_1 form during the $C_1 \rightarrow Q_1$ transition. Many X-ray diffraction studies (*3–5*) of the Q_2 form have been reported.

In the most recent works performed on single crystals, two structural models have been proposed with periodic antiphases in the Q_1 form (*6*). On the other hand, short-range order in $LiFeO_2$ has been found by X-ray diffusion and diffraction (*7–9*) as well as by electron diffusion (*10, 11*).

In this paper, we are concerned with the study of the Q_2 form by X-ray diffraction and transmission electron microscopy. These two complementary techniques have allowed us to select one of the two proposed structural models, to give a complete interpretation of twinning in the Q_2 form, to study the habit planes between crystals, i.e., between twins or families of twins, and to explain the characteristic features presented in single-crystal X-ray diffraction patterns.

B. Preparation of the Samples

The Q_2 form has been prepared from single crystals of the disordered C_1 form grown by the flux method described by An-

0022-4696/85 $3.00

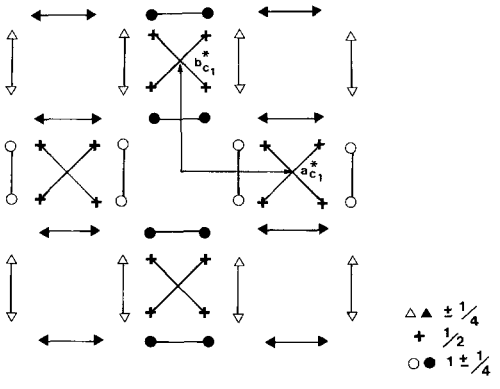

FIG. 1. Schematic representation of the satellite reflections and the diffuse streaks which bind them.

derson and Schieber (*12*). These crystals were annealed for 3 days at a temperature of 450°C giving a mixture of the Q_2 and C_1 forms. The transmission electron microscopy observations have been performed with a Jeol 100 CX microscope on fragments obtained by crushing these single crystals.

C. Description of the Q_2 Form, X-Ray Diffraction Patterns, and Study of the Twinning

A preliminary study of the Q_2 form by single-crystal X-ray diffraction confirmed and completed Brunel and de Bergevin observations (*6*).

The X-ray diffraction patterns of the Q_2 form are related to those of the Q_1 form. At first approximation and with a weak variation of the lattice parameters, differences are noticed mainly in the extinction of all the superlattice reflections such as $h + k = 2n + 1$ and in the occurrence of four satellites located on two perpendicular $\langle 110 \rangle^*_{C_1}$ type reciprocal directions, symmetrically around the absent reflection and at a distance of $\pm\frac{1}{4}r^*_{110_{C_1}}$ from it. Nearly continuous diffuse streaks connect couples of satellites on each $\langle 110 \rangle^*_{C_1}$ direction (Fig. 1). The fundamental reflections exhibit a fine structure with a lengthening at constant θ angle. This particularity has not been pointed out by Brunel *et al.* (Fig. 2). In order to explain their X-ray diffraction patterns, they proposed two structural models but could not distinguish between them.

The two models differ by the introduction of either one or two systems of periodic antiphase boundaries in the Q_1 structure. Depending on the model, these boundaries are parallel to one $\{110\}_{C_1}$ plane or to two perpendicular $\{110\}_{C_1}$ planes. In

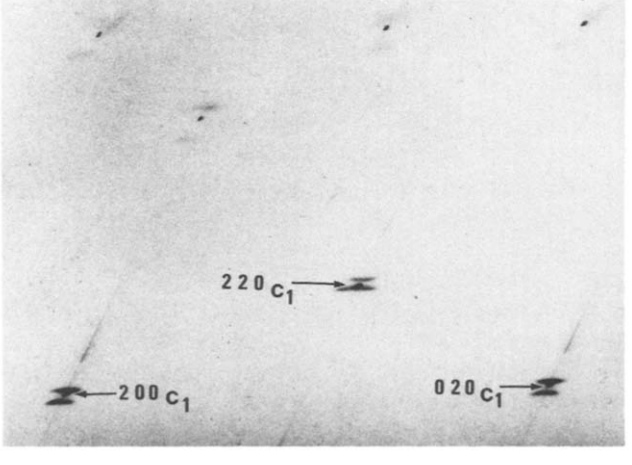

FIG. 2. Zero-level Weissenberg photograph $[001]_{C_1}$ rotation axis, $\lambda K_\alpha Cu$, width of the slit: 4 mm. Indices are related to the C_1 reflections.

TABLE I

MODULATION DIRECTIONS CHARACTERIZING THE A, B, C VARIANTS AND TWIN PLANES CONNECTING THEM IN THE MODEL WITH TWO DIRECTIONS OF MODULATION

Variants	Modulation directions	Twin planes	Connected variants
A	$[110]^*_{C_1}$ and $[1\bar{1}0]^*_{C_1}$	$(011)_{C_1}$ and $(0\bar{1}1)_{C_1}$	A – C
B	$[011]^*_{C_1}$ and $[0\bar{1}1]^*_{C_1}$	$(101)_{C_1}$ and $(10\bar{1})_{C_1}$	A – B
C	$[101]^*_{C_1}$ and $[10\bar{1}]^*_{C_1}$	$(110)_{C_1}$ and $(1\bar{1}0)_{C_1}$	B – C

both cases, they are 2 d_{110C_1} apart, conservative, and characterized by the antiphase vector $\mathbf{R} = \frac{1}{2}\langle 110\rangle_{C_1}$ parallel to the antiphase boundaries. It is worth noting that, for both models, the antiphase vectors affect the cation sublattice but do not change the anion sublattice insofar as it slightly deviates from a perfect cubic compact array.

For each model, the number and the orientation relations existing between these variants can be predicted.

(a) Model with Two Directions of Modulation

The Q_2 form structure has a tetragonal symmetry (space group $I4_1/amd$), the quaternary axis being parallel to the antiphase boundaries. The unit cell vectors can be expressed without deformation by

$$\mathbf{a}_t = 2\,\mathbf{a}_{C_1} - 2\,\mathbf{b}_{C_1}$$
$$\mathbf{b}_t = 2\,\mathbf{a}_{C_1} + 2\,\mathbf{b}_{C_1}$$
$$\mathbf{c}_t = 2\,\mathbf{c}_{C_1}$$

During the $C_1 \rightarrow Q_2$ transition, the point group changes from $m3m$ to $4/mmm$ resulting in a symmetry decrease. Three variants denoted A, B, C can appear. Table I indicates the symmetry planes relating the three variants as well as the two modulated directions that characterize them.

(b) Model with One Direction of Modulation

The Q_2 form structure has a monoclinic symmetry (space group $C2/c$), the binary axis being perpendicular to the antiphase boundaries. The unit cell vectors can be expressed without deformation by

$$\mathbf{a}_m = 2\,\mathbf{c}_{C_1}$$
$$\mathbf{b}_m = 2\,\mathbf{a}_{C_1} + 2\,\mathbf{b}_{C_1}$$
$$\mathbf{c}_m = \tfrac{1}{2}\,(\mathbf{a}_{C_1} - \mathbf{b}_{C_1}) - \mathbf{c}_{C_1}$$

During the $C_1 \rightarrow Q_2$ transition, the point group changes from $m3m$ to $2/m$ and consequently 12 variants can appear. Each variant is characterized by only one $\langle 110\rangle^*_{C_1}$ direction of modulation parallel to the binary axis. Thence, in reciprocal space, each of the six $\langle 110\rangle^*_{C_1}$ directions is common to two variants. Therefore, the 12 variants can be classed in three families denoted I, II, and III, each one being characterized by two perpendicular directions of modulation (see Table II). The symmetry planes connecting these three families are the ones which relate the A, B, C variants in the tetragonal description. Taking into account the Q_1 form structural characteristics, the antiphase boundaries can coincide with two possible atomic X or Y planes, these planes being the only ones that do not correspond by a lattice translation (Fig. 3). These two possibilities generate the variants characterized by the same direction of modulation.

We have completed this preliminary study of the Q_2 form by a X-ray powder pattern investigation. We have established that a doublet and a triplet correspond, respectively, to the disordered C_1 form with 200 and 220 lines. The observation is incompatible with a tetragonal deformation

TABLE II

MODULATION DIRECTIONS CHARACTERIZING THE VARIANTS AND TWIN PLANES CONNECTING THEM IN THE MODEL WITH ONE DIRECTION OF MODULATION

Families	Variants	Modulation directions	Twin planes	Connected variants
I	1 – 2	$[1\bar{1}0]^*_{C_1}$	$(1\bar{1}0)_{C_1}$ and $(001)_{C_1}$	1 – 2
	3 – 4	$[\bar{1}10]^*_{C_1}$	$(100)_{C_1}$	1 – 3
			$(010)_{C_1}$	1 – 4
II	1′ – 2′	$[011]^*_{C_1}$	$(0\bar{1}1)_{C_1}$ and $(100)_{C_1}$	1′ – 2′
	3′ – 4′	$[0\bar{1}1]^*_{C_1}$	$(010)_{C_1}$	1′ – 3′
			$(001)_{C_1}$	1′ – 4′
III	1″ – 2″	$[101]^*_{C_1}$	$(\bar{1}01)_{C_1}$ and $(010)_{C_1}$	1″ – 2″
	3″ – 4″	$[10\bar{1}]^*_{C_1}$	$(001)_{C_1}$	1″ – 3″
			$(100)_{C_1}$	1″ – 4″

but is in agreement with a monoclinic deformation of the anion sublattice. In addition, it confirms the remarks made by Lefebvre (*13*). The refinement of the monoclinic unit cell parameters reported by Brunel *et al.* has led to the values

$$a_m = 8.571 \pm 0.010 \text{ Å}$$
$$b_m = 11.589 \pm 0.014 \text{ Å}$$
$$c_m = 5.147 \pm 0.006 \text{ Å}$$
$$\beta_m = 145.70 \pm 0.04°.$$

As we will see later, we have also determined the parameters of the smallest monoclinic cell which is characteristic of the anion sublattice deformation. The use of this cell allows the indexing of the fundamental lines only (see Fig. 11).

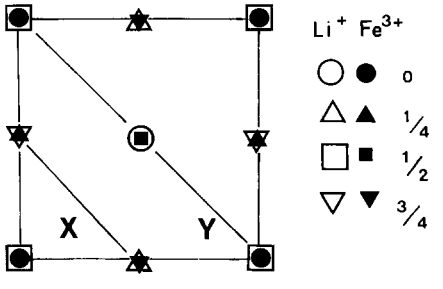

FIG. 3. (001) projection of the Q_1 structure. Only the cations are exhibited. X and Y atomic planes. Height expressed in the Q_1 basis.

$$\mathbf{a}'_m = \frac{\mathbf{a}_{C_1} - \mathbf{b}_{C_1}}{2}$$

$$\mathbf{b}'_m = \frac{\mathbf{a}_{C_1} + \mathbf{b}_{C_1}}{2}$$

$$\mathbf{c}'_m = \mathbf{c}_{C_1}.$$

That is

$$a'_m = 2.900 \pm 0.003 \text{ Å}$$
$$b'_m = 2.897 \pm 0.003 \text{ Å}$$
$$c'_m = 4.285 \pm 0.004 \text{ Å}$$
$$\beta'_m = 89.19 \pm 0.03°.$$

The preceding information was used to relate the observed fine structure of the fundamental reflections in Weissenberg photographs to the twinning of the samples. The following example shows the difficulties we have met in that attempt. Single-crystal X-ray diffraction patterns exhibit the existence of orientation crystallographic relations between the Q_2 and C_1 forms. As reported before, in the monoclinic model, there are 12 reflections corresponding to the 200_{C_1} reflection. Four of them have 002 indices related to the $\mathbf{a}'_m$, $\mathbf{b}'_m$, $\mathbf{c}'_m$ monoclinic cell. They are relative to 1′, 2′, 3′, 4′ variants of the II family and are characterized by a Bragg θ angle such as $\theta < \theta_{200C_1}$.

In the interpretation proposed by Brunel *et al.*, the $\mathbf{a}'_m$ and $\mathbf{c}'_m$ vectors characterizing

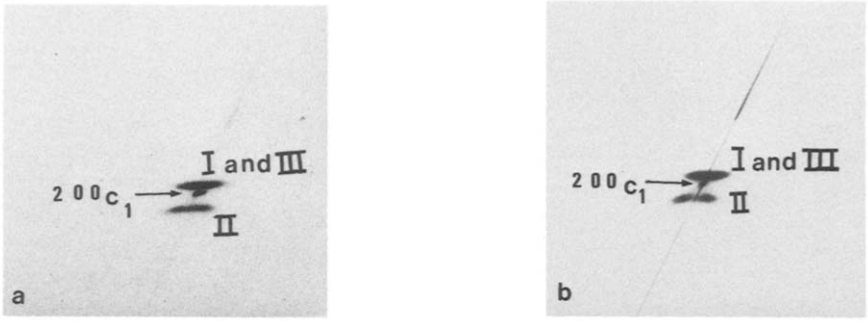

FIG. 4. Magnified part of the zero-level Weissenberg photograph shown in Fig. 2. (a) Slit of 4 mm, (b) slit of 0.3 mm.

each variant are necessarily located in a $\{110\}_{C_1}$ plane. Nevertheless the orientation of $\mathbf{a}'_m$ and $\mathbf{c}'_m$ vectors with respect to $\langle 110\rangle_{C_1}$ and $\langle 100\rangle_{C_1}$ directions are still undetermined. Two possibilities can be considered:

—If the $\mathbf{a}'_m$ vectors were strictly parallel to $\langle 110\rangle_{C_1}$ directions, the $\mathbf{c}'^*_m$ reciprocal vectors characterizing the variants of a same family would be superimposed and parallel to a $\langle 110\rangle^*_{C_1}$ direction. For a crystal oriented along $[001]_{C_1}$, the four reflections corresponding to the variants of the II family would be superimposed and located on the $[100]^*_{C_1}$ axis in the zero-level Weissenberg photograph.

—If the $\mathbf{a}'_m$ vectors were not exactly parallel to $\langle 110\rangle_{C_1}$ directions, the $\mathbf{c}'_m$ vectors corresponding to the variants of a same family would no longer be superimposed. In the case of the II family, their extremities would be located on the corners of a square centered on the $[100]^*_{C_1}$ axis, the diagonals of which are parallel to $[011]^*_{C_1}$ and $[0\bar{1}1]^*_{C_1}$ directions. For a crystal oriented along $[001]_{C_1}$, two pairs of 002 reflections would be symmetrically located above and below the zero-level Weissenberg photograph.

The $hk0_{C_1}$ Weissenberg photographs made with two different widths of the slit (4 and 0.3 mm) showed different behaviors. With the broad slit, the reflection was lengthened at constant θ angle. With the fine slit, there was an absence of intensity in the central part of this same reflection (Fig. 4).

These experimental observations are not consistent with either of the two assumptions just mentioned. They suggest a greater complexity in the orientation relations of the C_1 and Q_2 forms. A further study by electron microdiffraction and microscopy has allowed a complete description of this orientation.

D. Results and Discussion

(a) Choice between the Two Structural Models

Electron microscopy has shown the existence of large regions (of a few micrometers) characterized by the presence of either the C_1 or the Q_2 form. The diffraction patterns agree with the X-ray diffraction observations. A $(001)^*_{C_1}$ section of the Q_2 form reciprocal lattice is shown in Fig. 5, *a* and *b* points are, respectively, the intersection points of the observation plane with the diffuse streaks parallel to $[011]^*_{C_1}$ and $[01\bar{1}]^*_{C_1}$ directions on the one hand and parallel to $[101]^*_{C_1}$ and $[10\bar{1}]^*_{C_1}$ directions on the other hand. The pattern shown in Fig. 6 is obtained after a nearly 20° rotation from the $(001)^*_{C_1}$ plane about the $[100]^*_{C_1}$ direction. For higher diffraction angles, for example, in *c* points, the whole diffuse streaks can be observed.

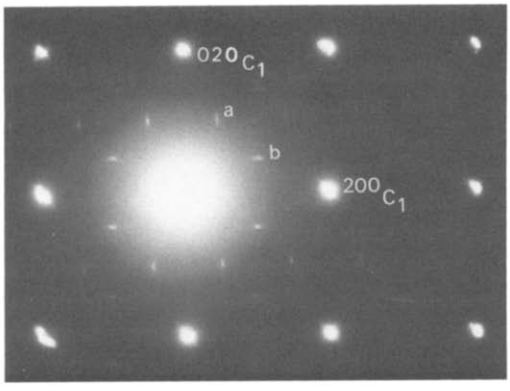

FIG. 5. $(001)^*_{C_1}$ section diffraction pattern · Intersection of the observation plane with: (in a point) the diffuse streaks parallel to $[011]^*_{C_1}$ and $[0\bar{1}1]^*_{C_1}$; (in b point) the diffuse streaks parallel to $[101]^*_{C_1}$ and $[10\bar{1}]^*_{C_1}$.

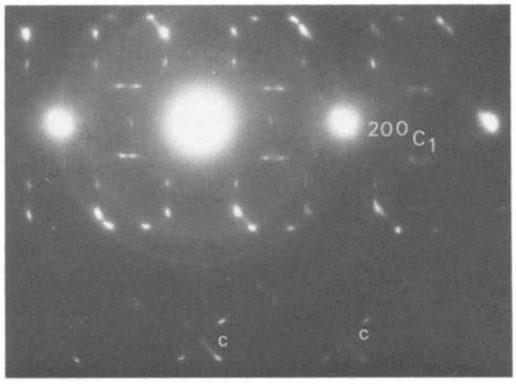

FIG. 6. Diffraction pattern obtained after a 20° rotation from $(001)^*_{C_1}$ about $[100]^*_{C_1}$.

In order to confirm the monoclinic model suggested by the Q_2 form's pattern, dark field images have been obtained by selecting two satellites located on two perpendicular directions of modulation. According to either structural assumption, such satellites belong or not to the same variant (see Tables I and II).

The dark field images shown in Figs. 7a and b illustrate our results. Each one reveals the existence of small domains (100 to 300 Å) limited by planes nearly parallel to

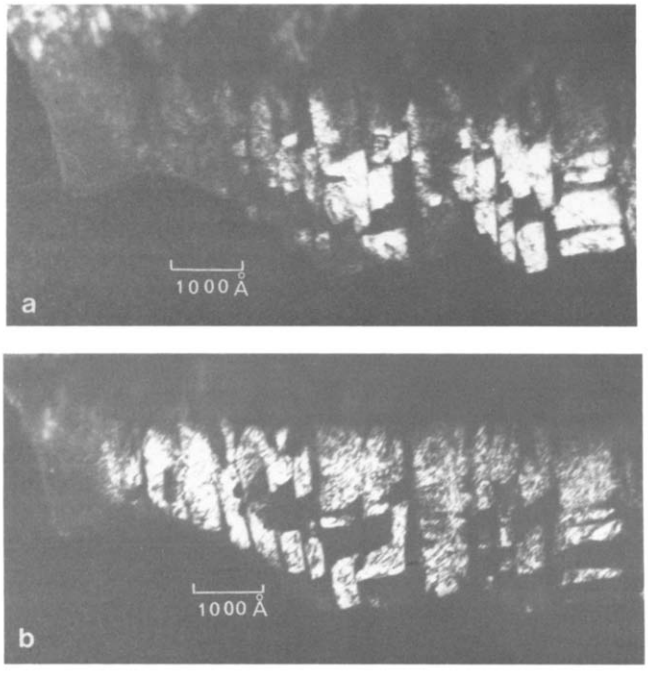

FIG. 7. Dark field images performed with the satellites. (a) $\bar{1} - \frac{1}{4}, -\frac{1}{4}, \frac{1}{2}$; (b) $\bar{1} - \frac{1}{4}, +\frac{1}{4}, \frac{1}{2}$. The indices are related to the C_1 basis. Observation plane: $(205)_{C_1}$.

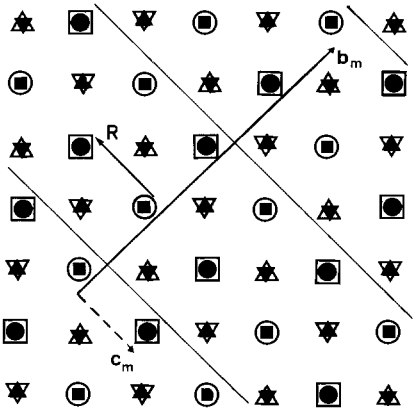

FIG. 8. Projection along $\mathbf{a}_m$ of the Q_2 monoclinic structure. Same symbols are used in Fig. 3. The antiphase boundaries are indicated with fine lines. The $\mathbf{c}_m$ extremity is located in $-\frac{1}{2}$.

$(100)_{C_1}$ and $(010)_{C_1}$. The domains in contrast in one dark field image correspond to the domains out of contrast in the other one. This means that the selected satellites for imaging the dark fields cannot belong to the same variant. This observation is sufficient to exclude the tetragonal model. Therefore the monoclinic model is the only one valid (Fig. 8). In Figs. 7a and b the domains in contrast correspond, respectively, to the 1–2 and 3–4 variants whereas the domains out of contrast correspond to the 3–4 and 1–2 variants (see Table II).

By the mere fact that these two micrographs or all the ones obtained under the same conditions are complementary, it can be deduced that the nucleation arises through the family of four variants. These families are the ones previously defined.

Inside a domain, the contrast is never uniform and varies with the magnitude of the diffuse intensity which is selected. The lattice images obtained by selecting two satellites of a same extinction reflection and the diffuse streak that binds them, show the existence of very irregular fringes (Fig. 9). These as well as the diffuse streaks parallel to $\langle 110 \rangle^*_{C_1}$ directions in the diffraction patterns suggest an imperfect order of the antiphase boundaries. The shortest distance measured between two fringes is 5.8 Å. This value is in good agreement with the

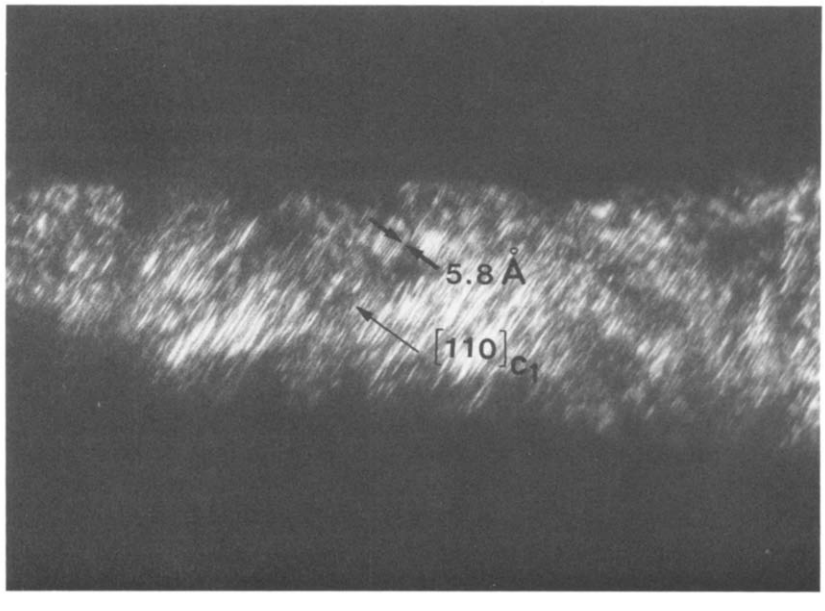

FIG. 9. Lattice image obtained by selecting two satellites and the diffuse streak which binds them.

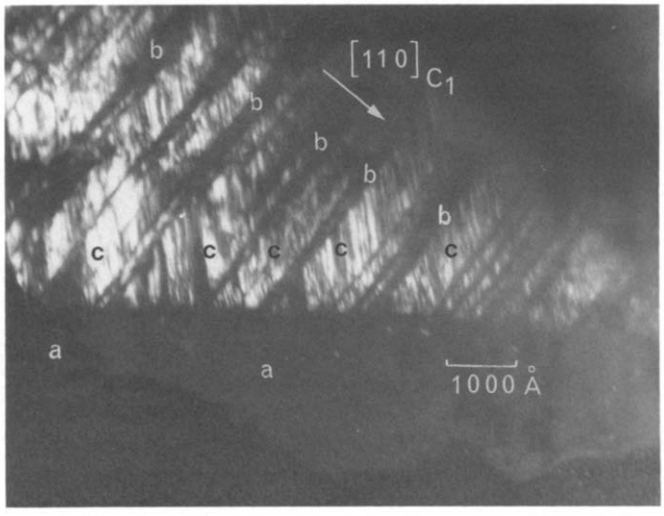

FIG. 10. Dark field image showing the three families disposition. Area a, I family; area b, II family; area c, III family. Observation plane: $(\bar{1}13)_{C_1}$.

expected 2 d_{110C_1} distance between antiphase boundaries.

(b) Study of the Habit Planes between Families of Four Variants

The dark field study has led to the following conclusions:

(1) The I, II, and III families coexist systematically and appear as bands with 100 to 800 Å width.

(2) Whatever the area we have investigated, two of the families exhibit a wide habit plane along a plane nearly parallel to $\{110\}_{C_1}$ and on the opposite develop very limited contacts with the third family.

These observations are shown in Fig. 10. This dark field image has been obtained by selecting the satellite reflection $1 - \frac{1}{4}, \frac{3}{2}, -\frac{1}{4}$ relative to the 1″ and 2″ variants of the III family. The I, II, and III families correspond, respectively, to the bands assigned by *a*, *b*, and *c*. The 1″ − 2″ and 3″ − 4″ variants in the *c* bands correspond, respectively, to the regions in contrast and out of contrast. Wide habit plane is observed between the II and III families along a $(110)_{C_1}$ plane.

Because of the small size of twin domains, the families of four variants form real entities for which habit planes have a physical meaning.

We have shown that the $C_1 \rightarrow Q_2$ transformation occurs with a monoclinic deformation of the anion sublattice. Based upon a cell with $\mathbf{a}_{C_1}$, $\mathbf{b}_{C_1}$, and $\mathbf{c}_{C_1}$, the deformation can be expressed by the tensor

$$\begin{vmatrix} e_1 & e_2 & e_4 \\ e_2 & e_1 & -e_4 \\ 0 & 0 & e_3 \end{vmatrix}$$ for the variant 1.

The e_i coefficients are easily calculated as shown in Fig. 11 with the previously de-

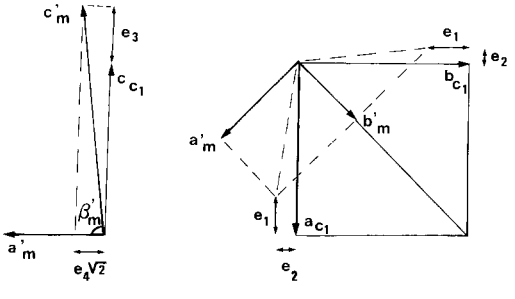

FIG. 11. Monoclinic cell: $\mathbf{a}'_m$, $\mathbf{b}'_m$, $\mathbf{c}'_m$. C_1 cubic cell: $\mathbf{a}_{C_1}$, $\mathbf{b}_{C_1}$, $\mathbf{c}_{C_1}$. The deformation is strongly magnified.

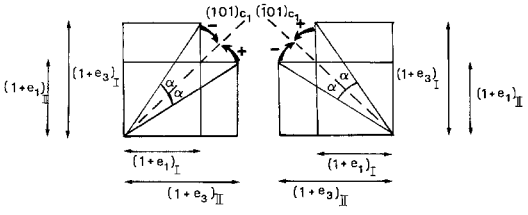

FIG. 12. Habit planes possibilities between the I and II families. The tetragonal deformation is strongly magnified.

fined a'_m, b'_m, c'_m, and β'_m parameters. They are given by

$$e_1 = \frac{a'_m + b'_m}{a_{C_1}\sqrt{2}} - 1 = -137 \times 10^{-4}$$

$$e_2 = \frac{a'_m - b'_m}{a_{C_1}\sqrt{2}} = -6 \times 10^{-4}$$

$$e_3 = \frac{c'_m \sin \beta'_m}{a_{C_1}} - 1 = 307 \times 10^{-4}$$

$$e_4 = \frac{c'_m \cos \beta'_m}{a_{C_1}\sqrt{2}} = 103 \times 10^{-4}.$$

The presence in the same proportions of different twin domains and their uniform repartition in the families involve a tetragonal macroscopic deformation for each family. For the I family, this deformation, referred to $\mathbf{a}_{C_1}$, $\mathbf{b}_{C_1}$, $\mathbf{c}_{C_1}$ axis, is expressed by the tensor

$$|e_{ij}|_t = \begin{vmatrix} e_1 & 0 & 0 \\ 0 & e_1 & 0 \\ 0 & 0 & e_3 \end{vmatrix}$$

obtained by averaging the four tensors associated to the four variants of this family. From the electron microscopy observations, it is deduced that the habit plane between two families of four variants can be formed in two different ways, that is to say along two perpendicular $\{110\}_{C_1}$ planes. These are the twin planes relating the involved families.

Referring to Fig. 12, it may be seen that the existence of a nondeformed $(101)_{C_1}$ or $(\bar{1}01)_{C_1}$ plane between the I and II families involves a $\pm\alpha$ rotation about the $[010]_{C_1}$ direction for both families. α is equal to $\pm (e_3 - e_1)/2$, its value is $\pm 0.022_2$ rads ($\pm 1.27°$).

The same conclusions apply to the I and III families as well as to the II and III families (Table III). This interpretation is in good agreement with our observations particularly because only two of the three families have a wide habit plane. It involves to distinguish six associations of two families with a nondeformed plane.

The possibilities of invariant elements between the Q_2 and C_1 forms have been examined in another way. In order to determine these invariant elements, one must consider the orientation relations between a family of four variants (for example, the I family) and the C_1 matrix or consider the cubic-tetragonal transformation corresponding to the $|e_{ij}|_t$ deformation previously defined. Since the e_1 and e_3 coefficients have opposite signs, this transformation can keep an invariant direction if one adds a $|\omega_{ij}|$ rotation such that the $|e_{ij}|_t + |\omega_{ij}|$ determinant is equal to zero (*14*).

Among all the rotations solving this equation, the ω rotation about the $[100]_{C_1}$ and $[010]_{C_1}$ directions, expressed by $\pm\sqrt{-e_1e_3}$, are equal to ± 0.020 rads ($\pm 1.17°$). This value is very close by the α rotation value previously determined (1.27°). In order to permit the I family to present simultane-

TABLE III

ROTATION AXIS FOR THE FAMILIES IN ORDER TO INDUCE THE EXISTENCE OF NONDEFORMED PLANES BETWEEN THEM

Connected families	Nondeformed planes	Rotation axis
I – II	$(101)_{C_1}$ $(10\bar{1})_{C_1}$	$[010]_{C_1}$
I – III	$(011)_{C_1}$ $(0\bar{1}1)_{C_1}$	$[100]_{C_1}$
II – III	$(110)_{C_1}$ $(1\bar{1}0)_{C_1}$	$[001]_{C_1}$

TABLE IV

RECIPROCAL COORDINATES OF REFLECTIONS DERIVING FROM THE 200_{C_1} REFLECTION

	Rotation axis	Rotation direction	Variants	x^*	y^*	z^*
I Family	$[010]_{C_1}$	$+\alpha$	1, 4	2.026	0	−0.064
			2, 3	2.027	0	−0.023
		$-\alpha$	1, 4	2.027	0	0.023
			2, 3	2.026	0	0.064
	$[100]_{C_1}$	$+\alpha$	1, 4	2.028	0	−0.020
			2, 3	2.028	0	0.020
		$-\alpha$	1, 4	2.028	0	−0.020
			2, 3	2.028	0	0.020
II Family	$[001]_{C_1}$	$+\alpha$	1′, 2′, 3′, 4′	1.934	0.044	0
		$-\alpha$	1′, 2′, 3′, 4′	1.934	−0.044	0
	$[010]_{C_1}$	$+\alpha$	1′, 2′, 3′, 4′	1.934	0	0.044
		$-\alpha$	1′, 2′, 3′, 4′	1.934	0	−0.044
III Family	$[100]_{C_1}$	$+\alpha$	1″, 3″	2.028	0.020	0
			2″, 4″	2.028	−0.020	0
		$-\alpha$	1″, 3″	2.028	0.020	0
			2″, 4″	2.028	−0.020	0
	$[001]_{C_1}$	$+\alpha$	1″, 3″	2.027	−0.023	0
			2″, 4″	2.026	−0.064	0
		$-\alpha$	1″, 3″	2.026	0.064	0
			2″, 4″	2.027	0.023	0

Note. For each variant, rotation axis and rotation direction are indicated.

ously an invariant direction with the C_1 matrix and a nondeformed $\{110\}_{C_1}$ plane with the II or III families, it is necessary that $\alpha = \omega$. In that way

$$\frac{e_3 - e_1}{2} = \sqrt{-e_1 e_3}.$$

This would involve $e_1 = -e_3$. But this condition is not in agreement with the measured deformation. The very small difference between α and ω (0.1°) makes it difficult to choose one of the two reported interpretations. Yet, for the areas characterized by the presence of the Q_2 form only, the first interpretation is the most probable.

(c) *Study of the Fine Structure of Fundamental Reflections Observed in Single-Crystal X-Ray Diffraction Patterns*

Whatever the interpretation we have chosen, each family of four variants has four possibilities of rotation. Consequently, the number of variants that could be present in the sample is 12 × 4, that is to say 48. The reciprocal coordinates calculation of the 48 reflections contributing to the intensity of each fundamental Q_2 reflections leads in both cases to very similar results which can explain their fine structure. We will restrict our presentation to the results concerning the fundamental Q_2 reflections

TABLE V

RECIPROCAL COORDINATES OF REFLECTIONS DERIVING FROM THE 220_{C_1} REFLECTION

	Rotation axis	Rotation direction	Variants	x^*	y^*	z^*
I Family	$[010]_{C_1}$	$+\alpha$	1, 2	2.028	2.029	−0.044
			3	2.026	2.026	−0.003
			4	2.025	2.026	−0.084
		$-\alpha$	1, 2	2.028	2.029	0.044
			3	2.025	2.026	0.084
			4	2.026	2.026	0.003
	$[100]_{C_1}$	$+\alpha$	1, 2	2.029	2.028	−0.044
			3	2.026	2.026	−0.003
			4	2.026	2.025	−0.084
		$-\alpha$	1, 2	2.029	2.028	0.044
			3	2.026	2.025	0.084
			4	2.026	2.026	0.003
II Family	$[001]_{C_1}$	$+\alpha$	1′, 4′	1.875	2.070	0
			2′, 3′	1.916	2.071	0
		$-\alpha$	1′, 4′	1.963	1.984	0
			2′, 3′	2.003	1.983	0
	$[010]_{C_1}$	$+\alpha$	1′, 4′	1.920	2.028	0.044; 0.042
			2′, 3′	1.959	2.028	0.045; 0.043
		$-\alpha$	1′, 4′	1.920	2.028	−0.042; −0.044
			2′, 3′	1.959	2.028	−0.043; −0.045
III Family	$[100]_{C_1}$	$+\alpha$	1″, 3″	2.028	1.959	0.045; 0.043
			2″, 4″	2.028	1.920	0.044; 0.042
		$-\alpha$	1″, 3″	2.028	1.959	−0.043; −0.045
			2″, 4″	2.028	1.920	−0.042; −0.044
	$[001]_{C_1}$	$+\alpha$	1″, 3″	2.071	1.916	0
			2″, 4″	2.070	1.875	0
		$-\alpha$	1″, 3″	1.983	2.003	0
			2″, 4″	1.984	1.963	0

Note. For each variant, rotation axis and rotation direction are indicated.

that are derived from the 200 and 220 reflections of the C_1 phase. The x^*, y^*, and z^* coordinates (Tables IV and V) have been computed with a value of α equal to $\pm 1.27°$ and a cell based upon the $\mathbf{a}^*_{C_1}$, $\mathbf{b}^*_{C_1}$, and $\mathbf{c}^*_{C_1}$ reciprocal vectors. Calculations and experimental observations are in good agreement.

These results can be illustrated by considering the 002 reflections of the II family reported in the first part of this paper (see Fig. 4).

The computed reflections are represented with a □ symbol in Fig. 13. From this figure, two types of observations would be expected on Weissenberg photographs made with a slit parallel to the $(001)^*_{C_1}$ plane.

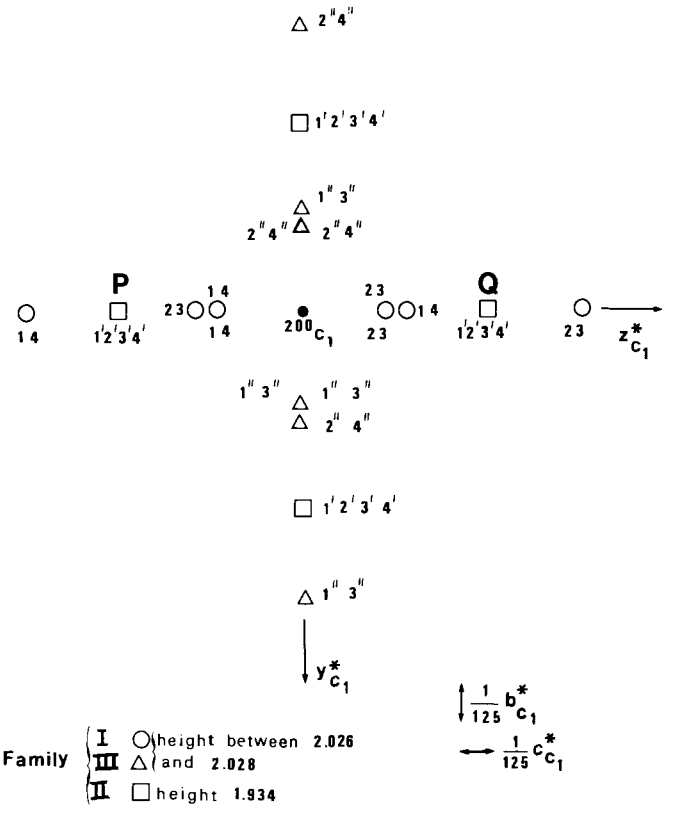

FIG. 13. Fine structure of the Q_2 fundamental reflection related to the 200_{C_1} reflection. The heights of the 48 reflections of I, II, and III families are expressed with respect to the $(100)^*_{C_1}$ plane crossing the origin. The numbers indicate the variants.

With a slit width larger than the reciprocal distance between the P and Q points, all the sixteen 002 reflections would appear. They would form a lengthened spot approximately parallel to the origin because the reflections situated at P and Q are not on the zero-level Weissenberg.

With a fine slit (width smaller than PQ), there should be no intensity in the central part of this reflection because the eight 002 reflections located on the $Oz^*_{C_1}$ axis are excluded. Indeed, these expected observations are observed experimentally (Figs. 4a and b).

E. Conclusions

The X-ray diffraction and transmission electron microscopy study has allowed us to choose between the two structural models reported by Brunel *et al.* for the metastable Q_2 form of $LiFeO_2$ ferrite. The monoclinic model with one direction of modulation is consistent with our observations.

The lowering of symmetry coming with the $C_1 \rightarrow Q_2$ transition involves the occurrence of a complex twinning, a complete analysis of which we have made. The nucleation arises by family of four variants, each of these families being characterized by two perpendicular directions of modulation. Because of the small size and the homogeneous repartition of twin domains in the three families, these families behave like real entities exhibiting an average tetragonal deformation.

Whatever the area we have investigated in the samples, any two families always develop between them a wide habit plane along a $\{110\}_{C_1}$ plane and exhibit very limited contacts with the third family. These conditions are realized because the families are rotated about two perpendicular $\langle 100\rangle_{C_1}$ directions. Each family has four possibilities of rotation and the number of monoclinic variants that could be present in the samples is equal to 48.

The reciprocal coordinate calculation of the 48 reflections that contribute to the intensity of each fundamental Q_2 reflections allows us to explain their fine structure and consequently to validate our interpretation.

References

1. E. Posnjack and T. Barth, *Phys. Rev.* **38,** 2234 (1931).
2. F. Barblan, E. Brandenberger, and P. Niggli, *Helv. Chim. Acta* **27,** 88 (1944).
3. R. Collongues, *C. R. Acad. Sci.* **241,** 1577 (1955).
4. M. Fayard, *Ann. Chim. (Paris)* **6,** 1279 (1961).
5. J. C. Anderson and M. Schieber, *J. Phys. Chem. Solids* **25,** 961 (1964).
6. M. Brunel and F. de Bergevin, *J. Phys. Chem. Solids* **29,** 163 (1968).
7. J. C. Anderson, S. K. Dey, and V. Halpern, *J. Phys. Chem. Solids* **26,** 1555 (1965).
8. M. Brunel and F. de Bergevin, *J. Phys. Chem. Solids* **30,** 2011 (1969).
9. M. Brunel, F. de Bergevin, and M. Gondrand, *J. Phys. Chem. Solids* **33,** 1927 (1972).
10. J. M. Cowley, *Acta Crystallogr. Sect. A* **29,** 537 (1973).
11. R. de Ridder, G. Van Tendeloo, D. Van Dyck, and S. Amelinckx, *Phys. Status Solidi A* **40,** 669 (1977).
12. J. C. Anderson and M. Schieber, *J. Phys. Chem.* **67,** 1838 (1963).
13. S. Lefebvre, thesis, Paris, 1975.
14. R. Bonnet and F. Durand, *Mater. Res. Bull.* **7,** 1045 (1972).